ELSEVIER

Cement & Concrete Composites 26 (2004) 873–881

Cement & Concrete Composites

www.elsevier.com/locate/cemconcomp

Electrical resistance change in compact tension specimens of carbon fiber cement composites

Farhad Reza [a,*], Jerry A. Yamamuro [b], Gordon B. Batson [c]

[a] Department of Civil Engineering, Ohio Northern University, 525 South Main Street, Ada, OH 45810, USA
[b] Department of Civil and Environmental Engineering, University of Delaware, Newark, DE 19716, USA
[c] Department of Civil and Environmental Engineering, Clarkson University, Potsdam, NY 13699, USA

Received 23 January 2003; accepted 4 June 2003

Abstract

The incorporation of a small volume of carbon fibers into a cement matrix can lead to multiple benefits including improvements in durability and tensile strength. In this paper, the smart material property of the composite which is its ability to respond to electrical stimuli was exploited. It was found that electrical resistance techniques which had previously been only applicable as investigative tools in fracture mechanics studies of metals could now be extended to the field of carbon fiber-reinforced concrete fracture mechanics. Compact-tension specimens of carbon fiber-reinforced mortar with volume percentages between 0% and 0.6% were tested. Fixed frequency electrical resistance measurements of 20 Hz, 100 Hz, 10 kHz and 1 MHz were taken during the tests. Good correlations between the electrical resistance behavior and mechanical behavior were observed. In particular, the electrical resistance may be used to provide some insight on the development and the mechanisms of the fracture process zone, and to provide an estimate of the length of a propagating crack. In addition, the tensile strength of the carbon fiber-reinforced mortar with 0.6% by volume of fibers increased by approximately three times over that of the unreinforced matrix.

Keywords: Electrical properties; Portland cement; Composite; Fiber reinforcement; Impedance

1. Introduction

Electrical resistance-based measurements have been used as investigative tools in the study of fracture mechanics of metals for many years. The electric potential method (EPM) was developed to aid in investigating crack growth in metals (see for example [1,2]) and an ASTM Standard exists for its use (ASTM E647). The operating principle is quite simple: the electrical field in a cracked specimen with a current flowing through it is a function of the specimen geometry, and in particular the crack size. For a constant current flow, the electric potential or voltage drop across the crack plane will increase with increasing crack size due to modification of the electrical field and associated perturbation of the current streamlines. The change in voltage can be related to crack size through analytical or experimental calibration curves. Assuming that the electrical resistivity remains constant, one could calculate the crack size a at any instant by using

$$a = \left[(a_f - a_0)\frac{(V - V_0)}{(V_f - V_0)}\right] + a_0 \tag{1}$$

In this equation, a_0 is the initial measured crack size, a_f is the final measured crack size, V_0 and V_f are the initial and final potential difference readings respectively and V is the instantaneous potential difference corresponding to crack size a. In lieu of using this expression which depends on an accurate measurement of the final crack size, one could use the following closed form equation derived by Johnson [1] and appearing in ASTM E647 for a compact tension (CT) geometry

$$\frac{a}{w} = \frac{2}{\pi}\cos^{-1}\left[\frac{\cosh(\pi Y_0/2w)}{\cosh\left[\frac{Y}{Y_0}\cosh^{-1}\left\{\frac{\cosh(\pi Y_0/2w)}{\cos(\pi a_0/2w)}\right\}\right]}\right] \tag{2}$$

In this equation, Y_0 is half of the distance between the voltage probes and w is as defined in Fig. 1.

Tada et al. [3,4] extended the application of the EPM to the problem of multiple small internal cracks in

* Corresponding author. Tel.: +1-419-772-2374; fax: +1-419-772-2404.
E-mail address: f-reza@onu.edu (F. Reza).

0958-9465/$ - see front matter © 2003 Elsevier Ltd. All rights reserved.
doi:10.1016/j.cemconcomp.2003.06.002

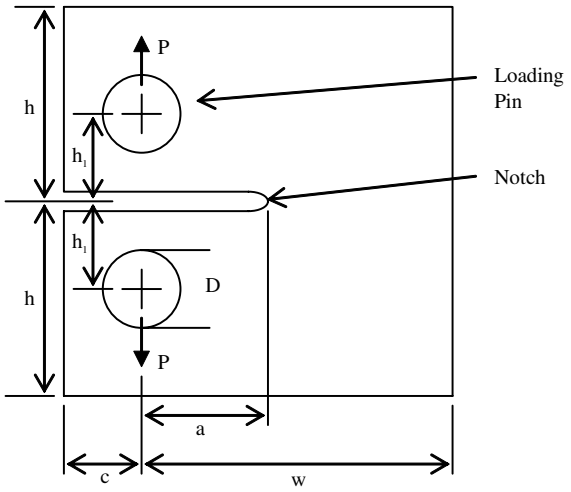

w = 203.2 mm (8 in)	
h = 121.9 mm (4.8 in);	h = 0.6w
h_1 = 55.9 mm (2.2 in);	h_1 = 0.275w
D = 50.8 mm (2 in);	D = 0.25w
c = 50.8 mm (2 in);	c = 0.25w
Thickness = 101.6 mm (4 in);	Thickness = 0.5w
a = 50.8 mm (2 in);	a = 0.25w

Fig. 1. Geometry of compact tension specimens.

metals. By utilizing the EPM and probabilistic inverse analysis, they determined volume crack densities. Petrenko and Gluschenkov [5] applied the EPM to measure crack velocities in ice.

It should be noted that in the application of EPM to fracture mechanics of metals, typically direct current (DC) is utilized. The ASTM Standard E647 allows the use of alternating current (AC) at low frequencies with the provision that the real resistance is used for correlations with crack length rather than the impedance. In other words the complex impedance should be resolved into a real resistance as well as imaginary reactance. The reason for the restriction on test frequency is that at higher frequencies there is a skin effect in metals where most of the current passes near the surface of the specimen rather than through the bulk of the material.

The study of electrical properties of concrete is quite advanced. Since the pioneering work of Hammond and Robson [6], investigators have looked at using electrical measurements for quality control [7] and assessment of corrosion levels [8] for example. Since it has long been recognized that DC measurements give rise to false polarization potentials in concrete [9], modern investigations almost exclusively utilize AC. Because concrete is heterogeneous consisting of several different phases and the interfaces between those phases, it is no surprise that the overall electrical response is frequency dependent. One widely accepted method of isolating the electrical conduction only through certain phases and interfaces is impedance spectroscopy. Several researchers have used this technique, for example, for microstructural characterization of concrete at various stages of hydration [10–12].

The use of electrical resistance in fracture mechanics studies of concrete has not received much attention until recently. Perhaps this is because the electrical resistance techniques were previously not believed to be readily applicable to concrete and because of the added complexity of the fracture problem in concrete. The concrete fracture problem is more complex than the metal problem in certain respects. Linear elastic fracture mechanics predicts that stresses can approach infinity at a sharp crack tip. This would imply catastrophic failure even with infinitesimal applied load. Since this is not the case in practice for real materials, a certain range of inelastic zone must exist at the crack tip. In metals, this inelastic zone is a yielding zone. In concrete, there are many complicated mechanisms acting around the crack tip. These mechanisms consume a part of the external energy caused by the applied load and thus can be regarded as toughening mechanisms. Typically the influences of each of these mechanisms are lumped together to define a conceptual fracture process zone.

One of the toughening mechanisms in the fracture process zone is microcracking. Due to the high stress state near the crack tip, microcracks develop at preexisting flaws. Such flaws result from water-filled pores, air voids and shrinkage cracks. In fiber-reinforced concrete, fiber bridging is also a toughening mechanism. After the matrix has cracked, the fibers can still transmit tensile stress across the two crack faces until the fibers pull out or break. Some other examples of toughening mechanisms are friction between crack faces resulting from the tortuous nature of the crack, crack-branching where secondary cracks develop from the main crack and aggregate bridging across the crack faces.

It is of much interest in the concrete fracture mechanics field to study experimental methods that may shed light on the length of a traction-free crack, the mechanisms of the fracture process zone, the size of the fracture process zone and how it varies with crack propagation. A discussion of various experimental techniques used in fracture mechanics of concrete is given by Shah et al. [13]. These techniques include laser holographic interferometry useful for monitoring surface crack propagation, acoustic emission useful for evaluating microcracking and dye penetration useful for evaluating crack shape across the thickness of the test specimen.

Chen and Chung [14] first reported that carbon fiber-reinforced concrete may have a smart material property, that is, the ability to sense damage. Recent investigations have shown that addition of carbon fibers to concrete gives the material a unique capability to respond to interrogation by electrical techniques [15,16]. Peled et al. [17] applied electrical measurements to fracture mechanics studies of carbon fiber-reinforced

mortar (CFRM). They performed investigations on double cantilever specimens using impedance spectroscopy techniques. The loading was stopped at various stages and the specimen subjected to a sweep in frequency (including DC). Based on the notion that DC resistance depended on the matrix only, and being able to identify the frequency at which only fibers contributed to conduction, they were able to predict uncracked, bridged and open area.

In the present investigation, electrical resistance measurements were recorded during fracture testing of CFRM. The tests were uninterrupted, that is, a continuous ramp function (displacement control) was used and electrical measurements were made at a fixed AC frequency. Compact tension geometry was utilized. Electrical resistance measurements were supplemented with displacement readings from several gages placed along the crack front. Good correlation was found between the electrical behavior and mechanical behavior. In particular, it was possible to identify process zone development and growth of the traction-free crack.

2. Experimental setup

The proportions used in preparing the base mixture for the CFRM specimens are shown in Table 1. Carboxy methylcellulose was added at a dosage of 1 kg/m^3 of the mixing water to aid in the dispersion of the carbon fibers. The use of a high quantity of silica fume and high-range water-reducing admixture is recommended for carbon fiber-reinforced concrete [18]. Since silica fume acts as a cement substitute, appropriate constituents were proportioned according to the total cementitious material content (that is, Portland cement plus silica fume) rather than just the cement content.

The cement was Type III Portland cement. The silica fume met ASTM 1240 requirements. The sand was ASTM C778 graded Ottawa sand. The high-range water-reducing admixture met the specifications of ASTM C494 Type A and F. The fibers used in this study were RK 10 carbon fibers. These were isotropic polyacrylonitrile (PAN)-based fibers of 8 μm diameter and 6 mm length. The fibers were coated with 1–2% sizing to keep multiple fibers together for ease of handling. The sizing was water-soluble and the fibers were readily dispersible in water.

Table 1
Mixture proportions for carbon fiber-reinforced mortar

Constituent	Content per unit volume of mortar (kg/m^3)	Ratio by weight to total cementitious material
Cement	632	0.87
Silica fume	95	0.13
Water	436	0.60
Sand	726	1.00
High-range water reducer	0–11	0.00–0.15
Methylcellulose	1 kg/m^3 of water	NA
Carbon fibers	0–1 vol.% of mortar	NA

Compact tension specimens were cast in a specially fabricated mold. The geometry of the CT specimens complied with that specified in ASTM E399 as described by Tada et al. [19]. The dimensions are indicated on Fig. 1. The CT specimens were cast as blocks 243.8 × 254 × 101.6 mm with two pin holes of 50.8 mm diameter. The load line location of the specimen is indicated on Fig. 1 by the tensile force, P. An initial notch of 101.6 mm was sawn into the specimen using a diamond blade that was approximately 3.2 mm thick. The notch was then sharpened by hand using successively finer diamond wire down to about 8 μm thickness. Thus, the initial notch length measured from the load line was 50.8 mm. The dimension w was 203.2 mm, thus the normalized initial crack length a/w was 0.25. The specimens were removed from the mold after 24 h and continuously moist cured until the day of the test. The specimens were allowed to dry for several hours prior to the test and all specimens had similar moisture conditions. Specimens were approximately 18 months old at the time of test.

A four-electrode configuration was utilized for the electrical measurements as depicted in Fig. 2. Current was supplied through the outer rings and potential difference was measured between the two inner rings. The potential sensing rings were placed approximately 50.8 mm apart from each other centered on either side of the notch. The electrodes were created by painting thin strips of silver paint around the specimen. Copper wire was then wound tightly over these strips. Electrical tape was used to enhance the contact between the copper wire and silver paint. The rings primarily served as the electrode while the silver paint ensured continuous contact around the specimen, even at the corners, which aided in creating uniform electric potential.

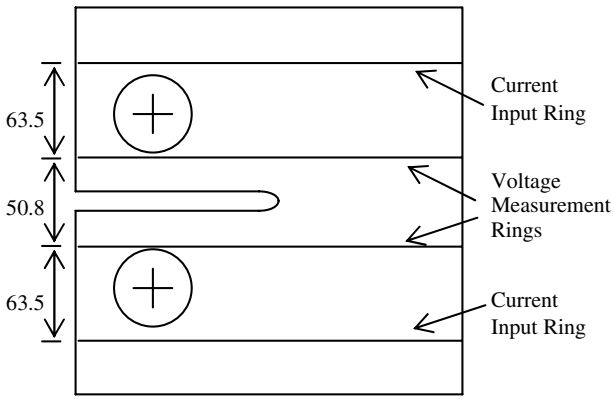

Fig. 2. Location of electrodes. Dimensions are in mm.

On both sides of the specimen, four linear variable differential transformers (LVDTs) were placed ahead of the expected path of the crack. Another LVDT was used to monitor crack mouth opening displacement (CMOD). For the purpose of identification, the LVDTs were numbered 1–4 sequentially with LVDT1 being the closest to the notch tip. Further, the notation 'f' was used for LVDTs on the front side and 'b' for those on the back side. Aluminum fixtures were used to hold the LVDTs. Acrylic blocks were also provided for the LVDTs to bear against. The fixtures were attached to the specimen using epoxy. The locations of the LVDTs are shown in Fig. 3. The CMOD gage had a range of ±2.54 mm while the other LVDTs had ranges of either ±1.02 or ±0.25 mm. The gage length for each LVDT was 114 mm.

Clevises for loading the specimen were fabricated out of stainless steel. The loading pins were made of high-strength aircraft aluminum. Special collars with ball bearings were used at each end of the pin. These ensured that the pins could rotate freely and would not bind up causing undesirable stresses in the specimen.

The fracture tests were performed on a 250-kN capacity closed loop control servo-hydraulic system. The tests were controlled by displacing the actuator (at the load line location) at a constant rate of 0.002 mm/s. Electrical resistance and reactance were measured using an inductance, capacitance, resistance (LCR) meter capable of testing at frequencies between 20 Hz and 1 MHz. A computer was utilized to simultaneously collect and synchronize resistance and reactance readings from the LCR meter, load and actuator displacement from the test frame as well as displacement readings from the 9 LVDTs coming through a signal conditioner. The experimental setup can be seen in Fig. 4. The figure shows a specimen secured in the loading clevises with the pins. The top clevis is attached to the load cell and the bottom clevis to the actuator. The figure also shows the four front LVDTs, the CMOD gage and the four electrodes around the specimen.

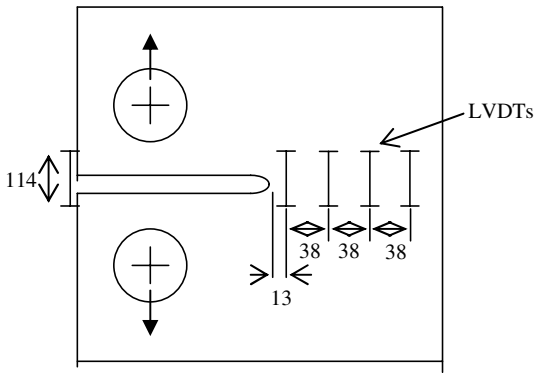

Fig. 3. Location of LVDTs. Dimensions are in mm.

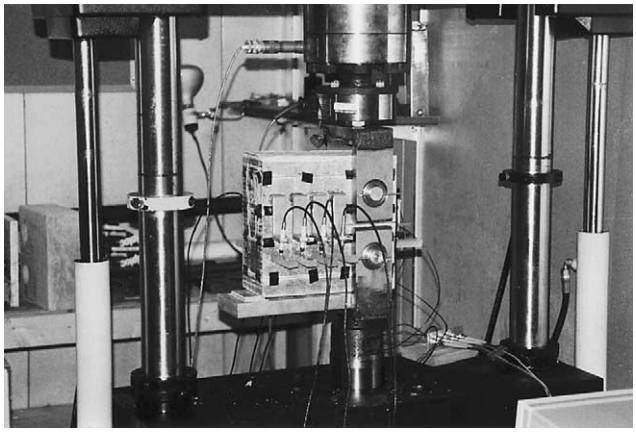

Fig. 4. Experimental setup.

3. Results

A total of 24 specimens were fracture tested including 6 specimens with no carbon fibers. The remaining 18 specimens were created with 0.2%, 0.4% or 0.6% by volume of carbon fibers. For a set of specimens with a particular volume of fibers, separate tests were conducted at AC frequencies of 20 Hz, 100 Hz, 10 kHz and 1 MHz.

The electrical resistance behavior during fracture tests from the plain mortar specimens proved not to be repeatable and hence these are not presented in the paper. It was concluded that no smart behavior was apparent for the plain mortar specimens.

Prior to fracture testing, impedance spectroscopy was performed on several specimens. The specimens were subjected to a sweep in test frequency between 20 Hz and 1 MHz. A typical test result for a specimen with 0.6% by volume of fibers is shown in Fig. 5. This plot of imaginary impedance (reactance) versus real impedance (resistance) is referred to as a Nyquist plot. Frequency increases from right to left on the graph. Only a single arc representing bulk electrical conduction could be seen. At low frequencies represented by the right hand side of the bulk arc, more of the electrical conduction is through the matrix than the fibers; at higher frequencies, more of the conduction is through the fibers than the matrix [20]. This is attributed to the development of a polarization layer of charge transfer resistance and double layer capacitance along the surface of the fibers. This serves to make the fibers insulating at low frequencies. At high frequencies, these layers vanish enabling the fibers to contribute significantly to the bulk electrical conduction. The absence of a secondary arc in Fig. 5 means that the frequency at which conduction is entirely through the fibers could not be determined. This implies that within this range of test frequencies, the measured bulk electrical conduction had contributions from both the matrix and the fibers.

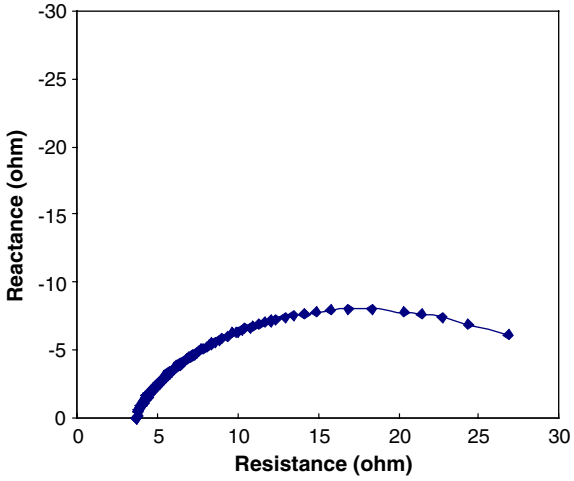

Fig. 5. Impedance spectroscopy of specimen containing 0.6% by volume of fibers.

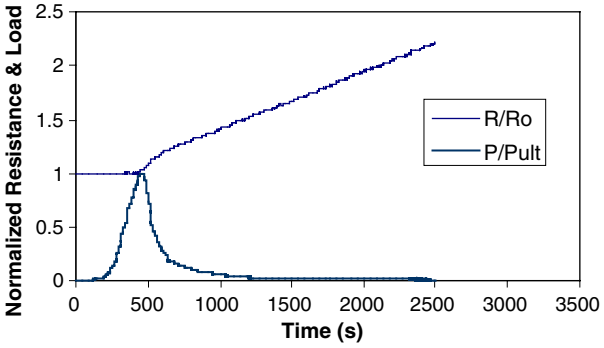

Fig. 6. Resistance and load versus time for specimen with 0.6% by volume of fibers tested at 1 MHz. Normalizing values were the initial resistance of 3.72 Ω and ultimate load of 12.45 kN.

In the discussion to follow, a somewhat idealized notion of the crack growth process is assumed. At any point in time, in the crack plane (that is the plane ahead of the original notch tip) there is an uncracked area where the matrix is intact and a cracked area. The cracked area may consist of both a physical crack and a fracture process zone. The physical crack is defined such that tensile stresses cannot be transmitted across the crack faces, in other words the faces are traction-free. The fracture process zone is assumed to lie ahead of the physical crack tip. The fracture process zone includes the toughening mechanisms of microcracking, fiber-bridging and other phenomena as discussed in the introduction.

Obviously, as the fracture test progresses the uncracked area decreases and the cracked area increases. It was hoped that the CFRM would act as a smart material and the resistance would be sensitive to these changes similar to resistance behavior in metals. In the traction-free portion of the crack there is no means of electrical conduction across the crack face. Therefore an increase in the traction-free area should logically cause the overall resistance to increase. In metals, the inelastic zone that develops is a yielding zone and this is not expected to change the resistance significantly. In other words, in metals the electrical resistance change is sensitive only to the growth of the traction-free crack and not the inelastic zone. The results obtained in this study showed that electrical resistance in the CFRM was responsive to the propagation of a traction-free crack but was also apparently sensitive to the fracture process zone.

The electrical resistance behavior at 1 MHz frequency during fracture testing for a specimen with 0.6% volume of fibers is shown in Fig. 6. The resistance values R have been normalized with respect to the initial resistance R_0 at the start of the test. It is observed that initially, there is little to no observable change in resistance. However, around time $t = 440$ s, a significant change occurs characterized by a nonlinear increase in resistance. This is followed by a period of approximately linear increase in resistance after approximately 600 s of elapsed time. For evaluative purposes the load versus time plot is superimposed on the graph. The load values P have been normalized with respect to the ultimate or peak load P_{ult}. The first increase in resistance occurs prior to peak load being achieved at approximately 97% of the ultimate load. The end of nonlinearity in the resistance behavior begins in the post peak region. Similar plots are shown in Figs. 7 and 8 for specimens tested at 10 kHz and 100 Hz respectively with 0.6% by volume of fibers. In Fig. 7, the first increase in resistance begins at time $t = 600$ s which corresponds to a load of 91% of the ultimate load. In Fig. 8, the first increase in resistance begins at time $t = 640$ s which corresponds to a load of 11% of the ultimate load.

It is hypothesized that the initial nonlinear increase in resistance may be associated with the development of the fracture process zone, while the linear portion may

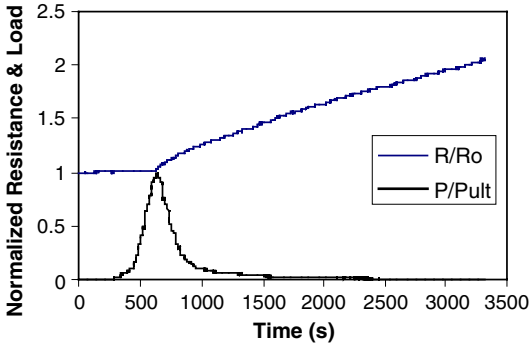

Fig. 7. Resistance and load versus time for specimen with 0.6% by volume of fibers tested at 10 kHz. Normalizing values were the initial resistance of 6.61 Ω and ultimate load of 12.32 kN.

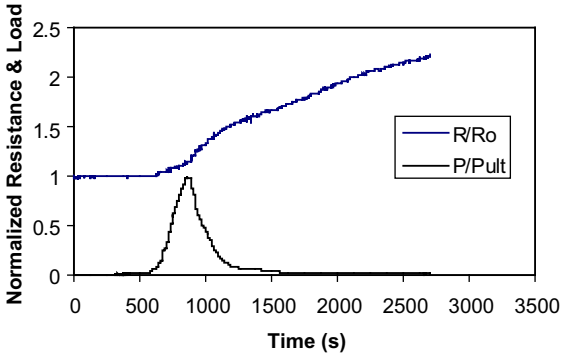

Fig. 8. Resistance and load versus time for specimen with 0.6% by volume of fibers tested at 100 Hz. Normalizing values were the initial resistance of 20.65 Ω and ultimate load of 12.84 kN.

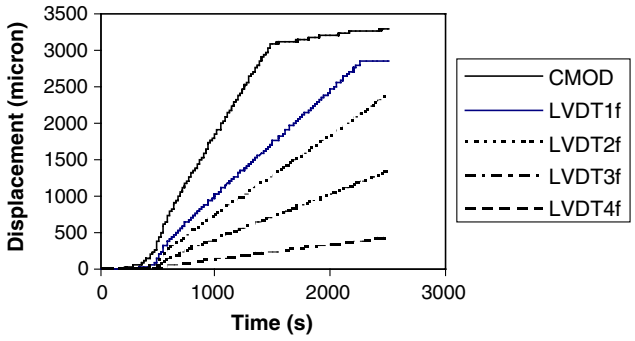

Fig. 9. Displacement versus Time for specimen with 0.6% by volume of fibers tested at 1 MHz.

be associated with growth of a traction-free crack. It was observed that the start of nonlinear increase in resistance appears to begin earlier in relation to the load value when measured at lower frequencies. This phenomenon may be due to microcrack coalescence ahead of the initial notch tip. Since the matrix contributes more to the overall bulk conduction at lower frequencies, the electrical resistance measurements are more sensitive to microcracking of the matrix than the higher frequency measurements. It appears that the readings at higher frequencies do not start increasing until fiber bridging in the fracture process zone has been initiated. This is because the fibers are more dominant in the bulk electrical conduction at higher frequencies. The fact that nonlinearity ends after the peak load may indicate that the process zone is not fully developed at the peak load but rather still growing. The final linear regime in the electrical behavior associated with the growth of the traction-free crack is similar to that observed in metals and hence many of the mathematical models relating crack length to resistance derived for metals may be applicable to concrete at this stage.

Fig. 9 shows the displacement versus time record obtained from the LVDTs for the same specimen used in Fig. 6, that is, the specimen tested at 1 MHz. In addition to the CMOD measurement, only the readings from the front gages are shown for the sake of clarity. At very large crack opening the CMOD and the displacement at LVDT1 exceed the range of the gage and this causes the observed flattening out of the curves. In general, three distinct patterns can be seen. Initially, there is little to no measured displacement. This is followed by a period of nonlinear increase in displacement which is probably induced by the fracture process zone and then a linear increase which likely indicates that the traction-free crack has progressed beyond this gage location. An enlarged view of this graph is shown in Fig. 10. The inelastic deformation is assumed to localize on the crack plane ahead of the physical notch tip. The nonlinear increase in resistance for the specimen tested at 1 MHz

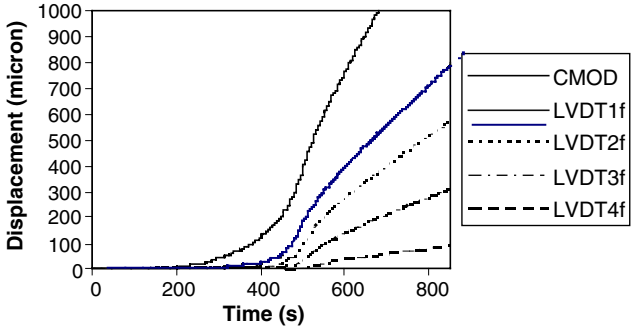

Fig. 10. Enlarged view of displacement versus time for specimen with 0.6% by volume of fibers tested at 1 MHz.

was found to begin approximately at time $t = 440$ s. From Fig. 10, it is observed that at time $t = 440$ s, the first gage ahead of the notch tip, that is LVDT1f, was already recording some activity. At this point the CMOD was 184 μm and the LVDT1 displacement was 46 μm. This seems to indicate that the process zone had already begun to develop. Fig. 11 shows a plot of the displacement record for the same specimen used in Fig. 8, that is the specimen tested at 100 Hz. The start of nonlinear increase in resistance was detected at approxi-

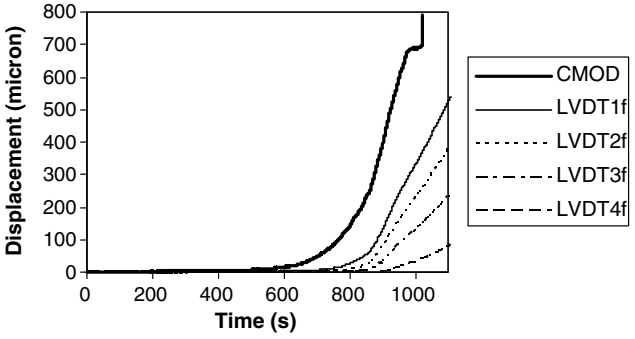

Fig. 11. Enlarged view of displacement versus time for specimen with 0.6% by volume of fibers tested at 100 Hz.

mately $t = 640$ s. Interestingly, from Fig. 11, it can be seen that this occurs roughly at the same time that the first gage ahead of the notch tip begins to detect some activity. The CMOD at this point was 22.8 μm and the LVDT1 displacement was only 3.65 μm. These results seem to indicate that electrical measurements at lower frequencies are more sensitive initially to the process zone development possibly because of microcrack coalescence in the fracture process zone which affects the matrix conductivity significantly but not the fiber conductivity. From the displacement records in Figs. 9–11, it is seen that the displacements all begin at zero and form a baseline in each graph. Starting with the crack tip gage, the displacements measured by each gage rise steadily leaving the baseline while the gages further from the original crack tip location remain on the baseline. From these graphs it appears that the crack tip is moving in a stable manner.

The crack profiles at various times during the fracture of the specimen tested at 1 MHz are shown in Figs. 12 and 13. Fig. 12 shows the record obtained from the front gages and Fig. 13 shows the record from the back gages. It is observed that after the peak load, that is after time $t = 500$ s (T500), the crack profile is reasonably linear. This observation is consistent with the approximately linear post-peak electrical resistance behavior which is associated with the growth of the traction-free crack. It is also observed that the gages on either side record similar activity, indicating that the crack growth (both physical crack and process zone) progresses approximately evenly along the sides, though it is not necessarily uniform across the width.

It follows that since the resistance is sensitive to crack propagation, it could be used to estimate crack length. One difficulty in being able to accurately monitor crack length in concrete that is common to any experimental technique is the tortuous nature of the crack growth. An example of this is shown in Fig. 14 for one of the test specimens. In the figure, the crack propagating from the original notch tip has been digitally enhanced for easy visual identification. Still, any technique that can provide an estimate of the crack length is a useful tool in fracture mechanics studies and has the potential to be applied to practical structures as well. The analytical expression relating crack length to resistance change given by Eq. (2) was used to obtain an estimate of the crack length. Fig. 15 shows the calculated normalized crack length and the normalized resistance change as a function of crack opening displacement measured by LVDT1 for the specimen tested at 1 MHz. It should be noted that it has been assumed that the CFRM obeys Ohm's law, therefore the normalized potential difference

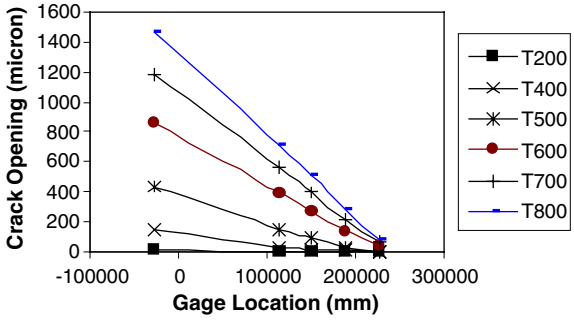

Fig. 12. Crack profile obtained from front gages for specimen with 0.6% by volume of fibers tested at 1 MHz.

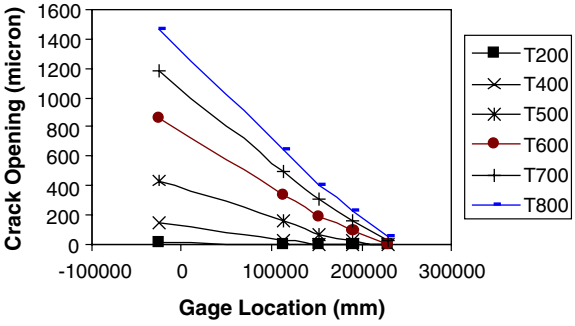

Fig. 13. Crack profile obtained from back gages for specimen with 0.6% by volume of fibers tested at 1 MHz.

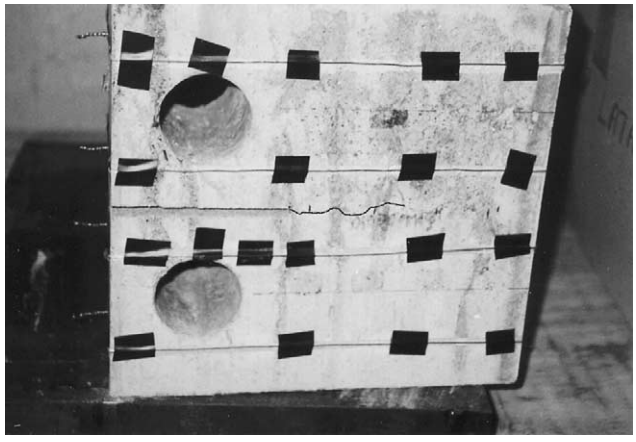

Fig. 14. Tortuous crack growth.

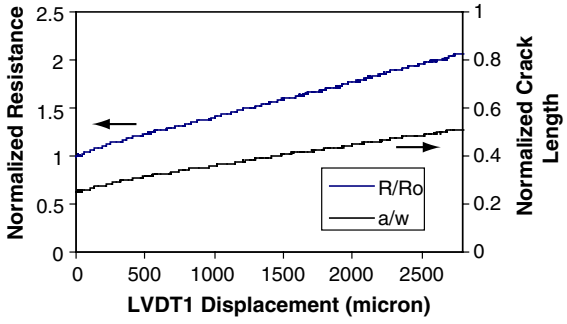

Fig. 15. Normalized resistance and crack length versus displacement for specimen with 0.6% volume of fibers tested at 1 MHz.

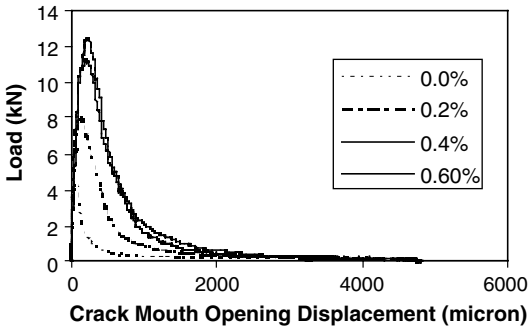

Fig. 16. Load versus crack mouth opening displacement for specimens containing various volumes of carbon fiber reinforcement.

V/V_0 is the same as the normalized resistance R/R_0. Also, Eq. (2) was derived for an initial normalized notch a/w of 0.25 which was the ratio used in these experiments. This is the value obtained when V/V_0 is 1. As seen in Fig. 15, the final resistance was approximately twice the initial value, and the estimated final crack length was also approximately double the starting value. The slight nonlinearity observed towards the beginning is believed to be due to the influence of the fracture process zone on the electrical resistance.

The addition of carbon fibers to a concrete matrix not only provides the material with the smart property discussed above but also leads to improvements in mechanical properties. One of the benefits of adding high modulus fibers to concrete is the increase in tensile strength over the unreinforced matrix. Fig. 16 shows typical load versus CMOD plots for CFRM specimens with increasing fiber volume content obtained from these experiments. There was almost threefold increase in tensile strength at 0.6% fiber volume content. Also, the tensile strain capacity of the composite was improved considerably.

4. Conclusions

Electrical resistance techniques have been and continue to be used as an aid in fracture mechanics studies of metals. These techniques had previously been inapplicable in the case of concrete. Recent investigations have shown a smart material capability in carbon fiber cement composites in that they are responsive to electrical interrogation schemes. In this paper, results from compact tension tests on carbon fiber-reinforced mortar specimens have shown that resistance techniques could potentially be used as an aid in the fracture mechanics studies of concrete. It was found that similar to the case of metals, resistance change was responsive to the growth of a traction-free crack and thus could be used to estimate crack length. Unlike the case of metals however, the resistance change was also found to be sensitive to the fracture process zone. In particular, resistance measurements made with low frequency current were sensitive to microcrack formation and high frequency measurements were sensitive to fiber bridging.

In addition to its use in fracture mechanics studies, electrical resistance might be a useful tool for monitoring crack growth in real structures. One potential application of this technique might be in concrete pavement management. Currently, several state transportation departments use a sophisticated digital image system to monitor and make decisions regarding pavement repair and design. This involves periodic photography of the pavement and subsequent use of pattern recognition software to evaluate crack growth by careful pixel-by-pixel superposition. Potentially, electrical resistance techniques could be used in remote sensing of the pavement. This could be more cost effective and would offer the advantage of real-time monitoring to capture the effect of moving loads, temperature changes, etc. on the crack growth.

Acknowledgements

This work was supported by the National Science Foundation under grant no. CMS-9522726. The authors also gratefully acknowledge the support of the following companies for their donation of materials to the research program: Globe Metallurgical Inc., of Niagara Falls, NY, who supplied the silica fume; and Master Builders Technologies of Cleveland, Ohio, who supplied the high-range water-reducing admixture. The authors also express their gratitude to Dr. John Dempsey at Clarkson University for allowing the use of the test equipment and facilities and for providing valuable advice.

References

[1] Johnson HH. Calibrating the electric potential method for studying slow crack growth. Mater Res Stand 1965;5:442–5.
[2] Saxena A. Electrical potential technique for monitoring subcritical crack growth at elevated temperatures. Eng Fract Mech 1980;13:741–50.
[3] Tada N, Kitamura T, Ohtani R. Probabilistic inverse analysis for predicting the distribution of multiple internal defects. Eng Fract Mech 1995;52:1015–27.
[4] Tada N, Hayashi Y, Kitamura T, Ohtani R. Analysis on the applicability of direct current electrical potential method to the detection of damage by multiple small internal cracks. Int J Fract 1997;85:1–9.
[5] Petrenko VF, Gluschenkov O. Crack velocities in freshwater and saline ice. J Geophys Res 1996;101(B5):11541–51.
[6] Hammond E, Robson TD. Comparison of electrical properties of various cements and concretes. The Engineer 1955;199:78–80, 114–115.
[7] Wilson JG, Whittington HW, Forde MC. Microprocessor-based system for automatic measurement of concrete resistivity. J Phys E: Sci Instrum 1983;16:700–5.

[8] Millard SG, Harrison JA, Gowers KR. Practical measurement of concrete resistivity. Br J Non-Destruct Test 1991;33(2):59–63.
[9] Monfore GE. The electrical resistivity of concrete. J PCA R&D Lab 1968;10(2):35–48.
[10] Christensen BJ, Coverdale RT, Olson RA, Ford SJ, Garboczi EJ, Jennings HM, et al. Impedance spectroscopy of hydrating cement pastes. J Am Ceram Soc 1994;77(11):2789–804.
[11] McCarter WJ, Brosseau R. The ac response of hardened cement paste. Cem Concr Res 1990;20:891–900.
[12] Gu P, Xie P, Beaudoin JJ, Brosseau R. AC impedance spectroscopy II: microstructural characterization of hydrating cement-silica fume systems. Cem Concr Res 1993;23:157–68.
[13] Shah SP, Swartz SE, Ouyang C. Fracture mechanics of concrete. John Wiley & Sons; 1995.
[14] Chen P, Chung DDL. Carbon fiber reinforced concrete as an intrinsically smart concrete for damage assessment during static and dynamic loading. ACI Mater J 1996;93(4):341–50.
[15] Reza F, Batson GB, Yamamuro JA, Lee JS. Volume electrical resistivity of carbon fiber cement composites. ACI Mater J 2001;98(1):25–35.
[16] Reza F, Batson GB, Yamamuro JA, Lee JS. Electrical resistance changes in carbon fiber cement composites undergoing compression. ASCE J Mater Civ Eng 2003;15(5):476–83.
[17] Peled A, Torrents JM, Mason TO, Shah SP, Garboczi EJ. Electrical impedance spectra to monitor damage during tensile loading of cement composites. ACI Mater J 2001;98(4):313–49.
[18] Banthia N. Carbon fiber cements: structure, performance, applications and research needs. In: Daniel JI, Shah SP, editors. Fiber reinforced concrete developments and innovations. Farmington Hills, MI: American Concrete Institute; 1994. p. 91–120.
[19] Tada H, Paris PC, Irwin GR. The stress analysis of cracks handbook. 2nd ed. St Louis, MO: Paris Productions; 1985.
[20] Torrents JM, Mason TO, Garboczi EJ. Impedance spectra of fiber-reinforced cement-based composites: a modeling approach. Cem Concr Res 2000;30(5):585–92.